

A simple chemosensor for ultrasensitive fluorescent “turn-on” detection of Fe³⁺ and alternant detection of CN⁻

Qin-Peng Zhang, Tai-Bao Wei, Jun-Nian An, Yan-Yan Chen, Guan-Fei Gong, Qi Zhou, Hai-Long Yang, Hong Yao, You-Ming Zhang & Qi Lin

To cite this article: Qin-Peng Zhang, Tai-Bao Wei, Jun-Nian An, Yan-Yan Chen, Guan-Fei Gong, Qi Zhou, Hai-Long Yang, Hong Yao, You-Ming Zhang & Qi Lin (2019): A simple chemosensor for ultrasensitive fluorescent “turn-on” detection of Fe³⁺ and alternant detection of CN⁻, *Supramolecular Chemistry*, DOI: [10.1080/10610278.2019.1690655](https://doi.org/10.1080/10610278.2019.1690655)

To link to this article: <https://doi.org/10.1080/10610278.2019.1690655>

 View supplementary material 

 Published online: 17 Nov 2019.

 Submit your article to this journal 

 Article views: 8

 View related articles 

 View Crossmark data 

ARTICLE



A simple chemosensor for ultrasensitive fluorescent “turn-on” detection of Fe³⁺ and alternant detection of CN⁻

Qin-Peng Zhang^a, Tai-Bao Wei^a, Jun-Nian An^a, Yan-Yan Chen^a, Guan-Fei Gong^a, Qi Zhou^a, Hai-Long Yang^a, Hong Yao^a, You-Ming Zhang^{a,b} and Qi Lin^a

^aKey Laboratory of Eco-Environment-Related Polymer Materials, Ministry of Education of China; Research Center of Gansu Military and Civilian Integration Advanced Structural Materials; College of Chemistry and Chemical Engineering, Northwest Normal University, Lanzhou, Gansu, P. R. China; ^bCollege of Chemistry and Chemical Engineering, Lanzhou City University, Lanzhou, Gansu, P. R. China

ABSTRACT

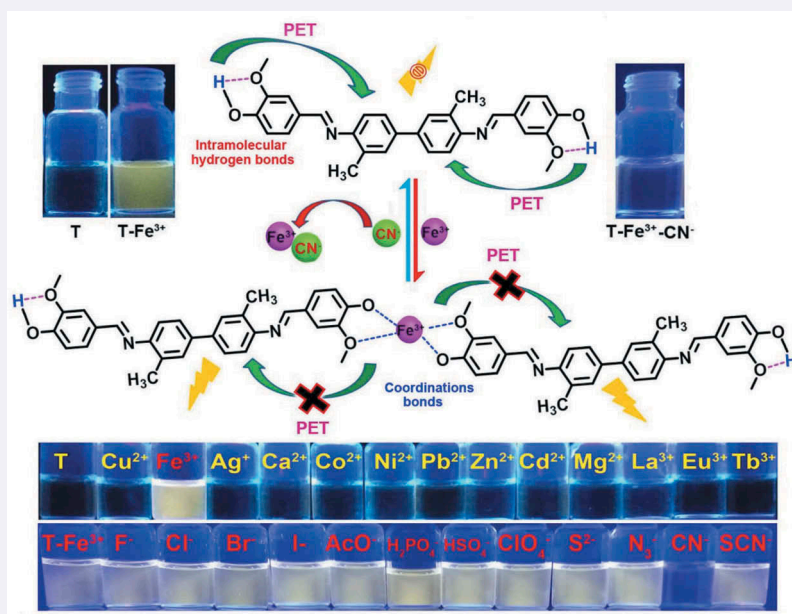
It is worth noting that Fe³⁺ is paramagnetic in nature. Thus, in most of the cases, Fe³⁺ behave as fluorescent quencher which makes it difficult to develop a fluorescent ‘turn-on’ chemosensor. Therefore, it is still a big challenge to devise and synthesise a simple chemosensor that could selectively detect Fe³⁺ via fluorescent ‘turn-on’ response. In this paper, A simple fluorescence chemosensor **T** based on N,N-(3,3-dimethyl biphenyl)-bis(2-methoxyphenol) has been synthesised. **T** could selectively detect Fe³⁺ via fluorescent ‘turn-on’ response. Meanwhile, the fluorescent spectrum limit of **T** towards Fe³⁺ was 0.178 nM, the detection limit was much lowest than previously reported fluorescent chemosensor and has reached to ultrasensitive level. In addition, **T** could also alternately detect CN⁻. Intriguingly, IMPLICATION logic gate was successfully constructed. Finally, the test papers and films based on **T** were prepared, which could be used as a fluorescent display material for the detection of Fe³⁺ and CN⁻.

ARTICLE HISTORY

Received 11 September 2019
Accepted 20 October 2019

KEYWORDS

Double schiff-base; detection of Fe³⁺ and CN⁻; dual-channel chemosensor; logic gate; test papers



In this article, a simple chemosensor (**T**) for ultrasensitive fluorescent ‘turn-on’ detection of Fe³⁺ and alternant detection of CN⁻ has been designed and synthesised. The fluorescent spectrum detection limit of **T** towards Fe³⁺ was 0.178 nM, the detection limit was much lowest than previously reported fluorescent chemosensor and has reached to ultrasensitive level. Based on the alternant detection property of **T** for Fe³⁺ and CN⁻, the fluorescent ‘ON-OFF-ON’ responding circle, IMPLICATION logic gate and test kits were constructed and prepared successfully, showing potential for practical applications in the detection of metal ions, toxic ions as well as smart material aspects.

CONTACT Tai-Bao Wei ✉ weitaobao@126.com; Qi Lin ✉ linqi2004@126.com ^aKey Laboratory of Eco-Environment-Related Polymer Materials, Ministry of Education of China; Research Center of Gansu Military and Civilian Integration Advanced Structural Materials; College of Chemistry and Chemical Engineering, Northwest Normal University, Lanzhou, Gansu 730070, P. R. China

Supplemental data for this article can be accessed [here](#).

© 2019 Informa UK Limited, trading as Taylor & Francis Group

Introduction

In the recent decade, the ultrasensitive detection of anions, cations and biomolecules has become increasingly important in the fields of food detection (1–3), clinical diagnostics (4–9), environmental monitoring (10–16), therefore, many scientists all over the world have been working in the area and developed numerous methods to achieve ultrasensitive detection of multi-analyte. For instance, Wu and co-workers designed and synthesised a conductive nanowire-mesh biosensor for ultrasensitive detection of serum reactive protein in Melanoma (17). Chattopadhyay and co-workers reported a lysosome-targetable fluorescent sensor for ultrasensitive detection of Hg^{2+} in living cells and real samples (18). Although chemists have been much successful at developing detection methods for multi-analyte, designing and developing a chemosensor that can recognise multi-analyte conveniently and efficiently is still a hot topic to be solved.

The detection of cations and anions has attracted more and more attention, due to they perform important roles in a wide range of biological and ecological systems. For example, Fe^{3+} , as one of the most important elements in metabolic processes, plays indispensable and versatile roles in a lot of biochemical processes at the cellular level for both human being and all the other biological worlds (19–23). In addition, the deficiency and excess of Fe^{3+} ions could cause many health problems in living organisms, such as heart disease, cancers, diabetes, anaemia and other dysfunction of organs (24–26). Moreover, anions are linked with various biological, environmental, pathological processes. Especially, cyanide ion is considered as a useful anion in many fields, including the fibre and resin manufacturing, metallurgy, and herbicide production. Although cyanide has important application value in chemistry and chemical industry fields, cyanide is also well known as a hazardous chemical in biological systems and the environment (27, 28). Therefore, it is of great theoretical and practical significance to explore high-efficiency and simple chemosensor for the quantitative detection of Fe^{3+} and CN^- in biological and environmental system.

In light of the above results and as part of our research interest in ion recognition field (29–32), we reported a simple and efficient chemosensor **T**, which could achieve the ultrasensitive detection of Fe^{3+} by fluorescent ‘turn-on’ response. In addition, **T** could not only detect Fe^{3+} but also detect CN^- successively. Based on the successive recognition property of **T**, the fluorescent ‘ON-OFF-ON’ responding circle and IMPLICATION logic gate were constructed by sequential addition of Fe^{3+} and CN^- into **T** solution. Moreover, the test kits and films loading **T** were prepared, which could be used as a fluorescent display material.

Experimental sections

Materials and instruments

All chemical reagents were commercially available at analytical grade and used without further purification. All solvents were purified and dried by standard methods. The cations were used from their perchlorate salts and purchased from Alfa Aesar Chemical Reagent. Meanwhile, the anions were used from their tetrabutylammonium (TBA) salts, which were purchased from Sigma Aldrich Chemical. Fresh double distilled water was used throughout the experiment. The ^1H NMR spectra were recorded on a Mercury-600 BB spectrometer at 600 MHz and a Mercury-400 BB spectrometer at 400 MHz, respectively. ^{13}C NMR spectra were recorded on a Mercury-600 BB spectrometer at 151 MHz and a Mercury-400 BB spectrometer at 101 MHz. The fluorescence spectra were recorded with a Shimadzu RF-5301 spectrofluorimeter. Ultraviolet–visible (UV–vis) spectra were recorded on a Shimadzu UV-2550 spectrometer. Mass spectra were recorded on a Bruker Esquire 6000 MS instrument. Melting points were tested on an X-4 digital melting-point apparatus. The infrared spectra were performed on Digilab FTS-3000 Fourier transform-infrared spectrophotometer. The morphologies and sizes of compound **T**, **T-Fe³⁺** and **T-Fe³⁺-CN⁻** were investigated using field emission scanning electron microscopy (FE-SEM, JSM-6701F).

General procedure for UV-vis experiments

All the UV-vis experiments were carried out in DMSO/ H_2O (8: 2, v/v) binary solution on a Shimadzu UV-2550 spectrometer. Any changes in the UV-vis spectra of the synthesised compound were recorded on addition of cations and anions while keeping the ligand concentration constant (2.0×10^{-4} M) in all experiments. Different cations (Fe^{3+} , Cu^{2+} , Ag^+ , Ca^{2+} , Co^{2+} , Ni^{2+} , Pb^{2+} , Zn^{2+} , Cd^{2+} , Mg^{2+} , La^{3+} , Eu^{3+} and Tb^{3+}) and anions (CN^- , F^- , Cl^- , Br^- , I^- , AcO^- , H_2PO_4^- , HSO_4^- , ClO_4^- , S^{2-} , N_3^- and SCN^-) were used for the UV-vis experiments.

General procedure for fluorescence spectra experiments

All the fluorescent spectroscopy was carried out in DMSO/ H_2O (8: 2, v/v) binary solution on a Shimadzu RF-5301 spectrometer. Any changes in the fluorescence spectra of the synthesised compound were recorded on addition of cations and anions while keeping the ligand concentration constant (2.0×10^{-4} M) in all experiments. Different cations (Fe^{3+} , Cu^{2+} , Ag^+ , Ca^{2+} , Co^{2+} , Ni^{2+} , Pb^{2+} , Zn^{2+} , Cd^{2+} , Mg^{2+} , La^{3+} , Eu^{3+} and Tb^{3+}) and anions (CN^- ,

F⁻, Cl⁻, Br⁻, I⁻, AcO⁻, H₂PO₄⁻, HSO₄⁻, ClO₄⁻, S²⁻, N₃⁻ and SCN⁻) were used for the fluorescent experiments.

Synthesis and characterisation of chemosensor **T**

The chemosensor **T** was synthesised by 4-hydroxy-3-methoxybenzaldehyde (0.684 g, 4.5 mmol), 3,3'-dimethylbenzidine (0.425 g, 2.0 mmol) and acetic acid (2 mL) were dissolved in absolute ethanol (60 mL), the reaction mixture was stirred under reflux for 12 h at 85°C. At the end of reaction, the rufous solution was obtained and extracted with dichloromethane, then dichloromethane layer was dried under vacuum to obtain a yellow powder, the yellow powder was recrystallised with ethanol to give a yellow powder product **T** (0.8068 g) in 84% yield. The melting point of compound **T** is over 300°C. ¹H NMR (CDCl₃, 600 MHz, room temperature) δ (ppm): 8.30 (s, 2 H), 7.65 (d, J = 1.8 Hz, 2 H), 7.48 (d, J = 2.1 Hz, 4 H), 7.30 (dd, J = 8.1, 1.8 Hz, 2 H), 6.99 (dd, J = 9.3, 8.0 Hz, 4 H), 5.96 (s, 2 H), 4.0 (s, 6 H), 2.43 (s, 6 H). ¹³C NMR (CDCl₃, 151 MHz) δ/ppm: 158.79, 150.28, 148.82, 147.03, 137.91, 132.09, 129.50, 128.69, 125.07, 124.81, 118.19, 114.16, 108.60, 56.07, 18.06. ESI-MS m/z: calcd for C₃₀H₂₈N₂O₄ [**T**+H]⁺: 481.2122; found: 481.21216.

Calculation formula of LOD

Linear Equation: Y = aX + b

$$\delta = \sqrt{\frac{\sum(F_i - F_0)^2}{N - 1}} \quad (N = 20)$$

LOD = K × δ/S (K = 3, S = a × 10⁶)

F₀ is fluorescence intensity of **T**, F_i is the average of fluorescent intensity F₀.

Results and discussion

As shown in Figure 1, the chemosensor **T** was synthesised and characterised by ¹H NMR, ¹³C NMR and ESI-MS (Figure S1-S3). Next, to ascertain the optimum water content system of **T** solution, the fluorescent experiment of different volume fractions of water content was carried out. Because

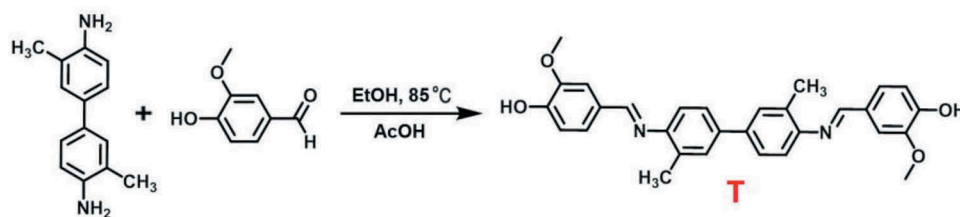


Figure 1. (colour online) Synthesis of chemosensor **T**.

the DMSO is a good solvent for **T** while water is a poor solvent for **T**, as shown in Figure S4, upon the addition of water into the DMSO solution of **T** with the increase of the water volume fractions, the fluorescent emission intensity at 528 nm reached the strongest state when the water volume fraction was at 20%. However, when the water contents exceeded 20%, the fluorescence intensity of **T** was decreased, which could be attributed to the formation of precipitate when more water was added into the **T** (water fractions 20%) solution. Based on above these results, we chose the solvent composition of DMSO/H₂O (8:2, v/v) to investigate fluorescent property of **T** in throughout the experiment. Subsequently, the recognition properties of the chemosensor **T** towards various metal ions (including Fe³⁺, Cu²⁺, Ag⁺, Ca²⁺, Co²⁺, Ni²⁺, Pb²⁺, Zn²⁺, Cd²⁺, Mg²⁺, La³⁺, Eu³⁺ and Tb³⁺) were investigated by UV-vis and fluorescent spectra in DMSO/H₂O (8:2, v/v) binary solution.

First, in the UV-vis spectra, with 5.0 equiv Fe³⁺ was added into **T** solution (2.0 × 10⁻⁴ M), the absorption peaks at 285 nm and 305 nm increased obviously (Figure 2), while the one at 363 nm decreased significantly, and accompanied by the solution colour change from pale yellow to colourless. The absorption peaks change may be ascribed to the newly formed complex between **T** and Fe³⁺. In comparison, other cations no obvious changes were observed in colour (inset of Figure 2). Furthermore, to confirm the selectivity of **T** towards Fe³⁺, the competitive experiment was implemented by adding 5.0 equiv various metal ions (including Cu²⁺, Ag⁺, Ca²⁺, Co²⁺, Ni²⁺, Pb²⁺, Zn²⁺, Cd²⁺, Mg²⁺, La³⁺, Eu³⁺ and Tb³⁺) into the mixed solution of **T** and Fe³⁺ respectively. The results showed that these competitive metal ions exerted no influence on the detection of Fe³⁺ (Figure 3).

Second, in the fluorescent spectra, when 5.0 equiv various (Fe³⁺, Cu²⁺, Ag⁺, Ca²⁺, Co²⁺, Ni²⁺, Pb²⁺, Zn²⁺, Cd²⁺, Mg²⁺, La³⁺, Eu³⁺ and Tb³⁺) metal ions were added into **T**, **T** and **T**+ other cations showed very weak fluorescence (Figure 4). However, upon the addition of 5.0 equiv Fe³⁺ into **T** solution, **T** emitted brilliant yellow fluorescence at 528 nm, which could be distinguished by naked-eyes under the irradiation of a portable UV-lamp

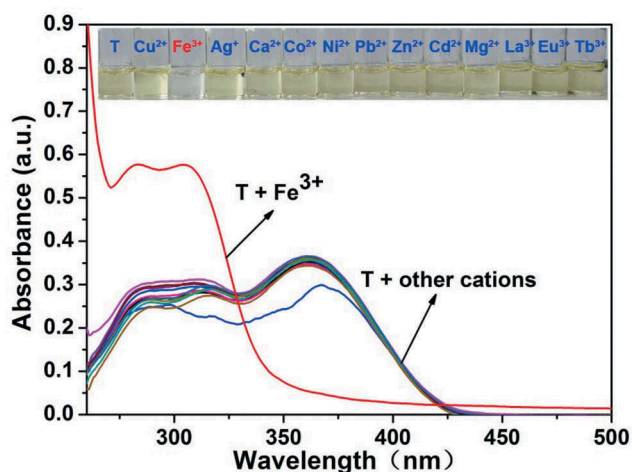


Figure 2. (colour online) UV-vis absorption spectra of chemosensor **T** (2×10^{-4} M) in DMSO/H₂O (8: 2, v/v) binary solution in the presence of Fe³⁺ and other cations (5.0 equiv.). Inset: Colour changes observed at natural light after 5.0 equiv. various cations were added into **T**.

(365 nm). In addition, to validate the selectivity of **T** for Fe³⁺, the control experiment was carried out by adding other competitive metal ions into the mixed solution of **T** and Fe³⁺ respectively. As a result, other competitive cations could not induce any obvious changes for the detecting process of Fe³⁺ (Figure 5). Therefore, **T** showed specific fluorescent selectivity towards Fe³⁺ in DMSO/H₂O (8: 2, v/v) binary solution.

To further explore the detection property of chemosensor **T** towards Fe³⁺ in DMSO/H₂O (8: 2, v/v) binary solution, UV-vis and fluorescent titration experiments were carried out. In the UV-vis titration experiments

(Figure 6). Upon sequential addition of Fe³⁺ (0–0.18 equiv.) into **T** solution (2.0×10^{-4} M), the absorption peaks at 285 nm and 305 nm increased gradually, while the one at 363 nm decreased, which could be attributed to the formation of coordination bonds between Fe³⁺ and oxygen atoms of **T**. As a result, this led to obvious colour change from pale yellow to colourless, which could be observed by the naked eyes (inset of Figure 2). The detection limit of UV-vis spectra changes for Fe³⁺ was calculated to be 1.58 nM on the basis of the $3\delta/S$ method (Figure S5). In the fluorescent titration experiment (Figure 7), the emission intensity of **T** at 528 nm was enhanced progressively with the increasing concentration of Fe³⁺ (0–0.18 equiv.), which could be caused by the inhibition of PET process due to the formation of coordination bonds between Fe³⁺ and oxygen atoms of **T** (forming the complex **T-Fe³⁺**). Moreover, the detection limit of fluorescent spectra changes for Fe³⁺ was 0.178 nM (Figure S6). It is worth noting that the fluorescent detection limit of **T** for Fe³⁺ was lowest than previously reported fluorescent chemosensor (Table 1) (33–41), corroborating that chemosensor **T** could achieve ultrasensitive detection of Fe³⁺ in DMSO/H₂O (8: 2, v/v) binary solution.

Then, the successive recognition property of **T-Fe³⁺** towards various anions (CN⁻, F⁻, Cl⁻, Br⁻, I⁻, AcO⁻, H₂PO₄⁻, HSO₄⁻, ClO₄⁻, S²⁻, N₃⁻ and SCN⁻) was further investigated by UV-vis experiment in DMSO/H₂O (8: 2, v/v) binary solution. In the UV-vis experiments (Figure S7), when 5.0 equiv CN⁻ was added into **T-Fe³⁺** solution (2.0×10^{-5} M), the absorption peaks of **T-Fe³⁺-CN⁻** at 285 nm and 305 nm declined obviously, while the one at 363 nm increased sharply. Subsequently, the control experiments were

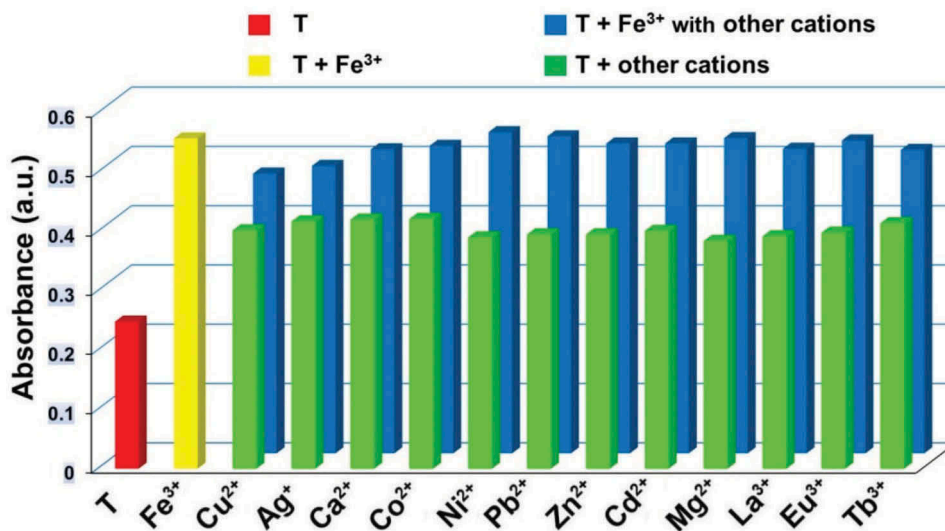


Figure 3. (colour online) UV-vis absorption histogram of chemosensor **T** with addition of 5.0 equiv. Fe³⁺ in the presence of various cations in DMSO/H₂O (8: 2, v/v) binary solution ($\lambda_{em} = 285$ nm).

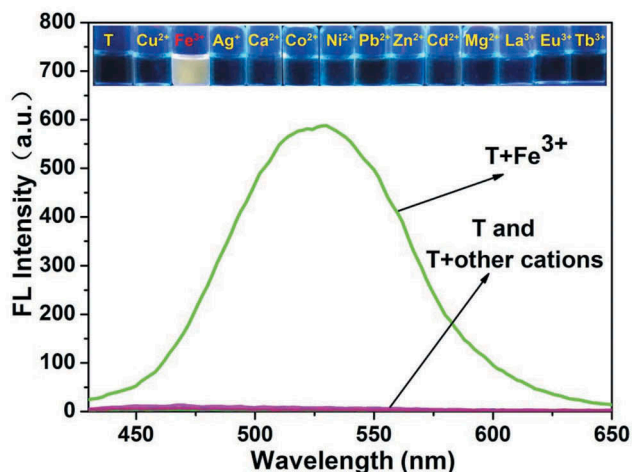


Figure 4. (colour online) Fluorescent emission spectra of chemosensor **T** (2×10^{-4} M) in DMSO/H₂O (8: 2, v/v) binary solution in the presence of Fe³⁺ and other cations (5.0 equiv.) ($\lambda_{\text{ex}} = 390$ nm). Inset: Colour changes observed at UV lamp (365 nm) after 5.0 equiv. various cations were added into **T**.

performed to investigate the selectivity of **T-Fe³⁺** for CN⁻ under the competition conditions. As shown in Figure S8, other competitive anions could not cause any obvious change for the detection process of CN⁻. In addition, UV-vis titration experiment was implemented to probe the detection property of **T-Fe³⁺** for CN⁻. As shown in Figure S9, the UV-vis spectrum detection limit of **T-Fe³⁺** towards CN⁻ was calculated to be 35.20 nM in UV-vis spectra.

Moreover, the fluorescent experiment was also utilised to investigate successive recognition property of **T-Fe³⁺** towards different anions (CN⁻, F⁻, Cl⁻, Br⁻, I⁻, AcO⁻, H₂PO₄⁻, HSO₄⁻, ClO₄⁻, S²⁻, N₃⁻ and SCN⁻) in DMSO/H₂O (8: 2, v/v) binary solution. As shown in Figure 8, the fluorescence of **T-Fe³⁺** was quenched

(inset of Figure 8) after 5.0 equiv CN⁻ was added into **T-Fe³⁺** solution, and other anions could not induce same fluorescent changes. In order to verify the selectivity of **T-Fe³⁺** towards CN⁻, the control experiments were carried out by adding various anions into **T-Fe³⁺** solution, respectively. The results showed these anions could not induce any interference for the CN⁻ sensing process (Figure 9). Meanwhile, to further explore the detection property of **T-Fe³⁺** for CN⁻, fluorescent titration experiment was also carried out. As shown in Figure S10, with the increasing concentration of CN⁻ (0–9.80 equiv.), the fluorescent emission intensity at 528 nm decrease gradually, which indicated PET interaction was recovered. Meanwhile, the fluorescent spectrum detection limit of **T-Fe³⁺** towards CN⁻ was obtained to be 206 nM on the basis of $3\delta/5$ method.

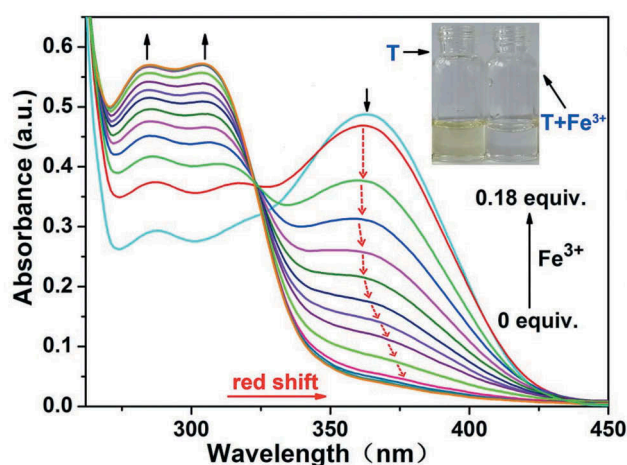


Figure 6. (colour online) UV-vis titration spectra of chemosensor **T** with increasing concentrations of Fe³⁺.

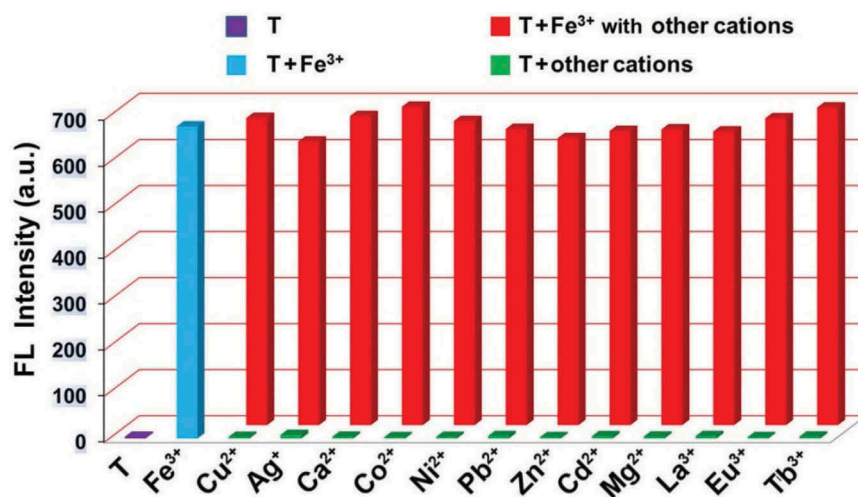


Figure 5. (colour online) Fluorescent histogram of chemosensor **T** with addition of 5.0 equiv. of Fe³⁺ in the presence of various cations in DMSO/H₂O (8: 2, v/v) binary solution ($\lambda_{\text{ex}} = 390$ nm, $\lambda_{\text{em}} = 528$ nm).

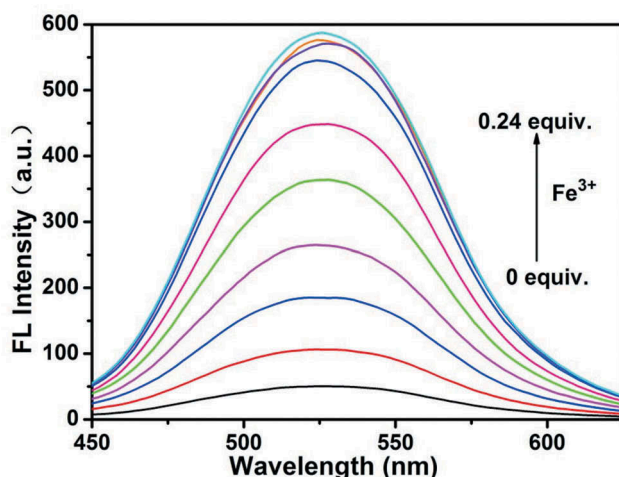


Figure 7. (colour online) Fluorescent titration spectra of chemosensor **T** with increasing concentrations of Fe^{3+} .

Table 1. Comparison of detection limit of different fluorescent chemosensors for Fe^{3+} .

Fluorescent Chemosensors	Detection Limit (nM)	Ref
N/P codoped carbon dots	330.0	(33)
Nitrogen and phosphorus codoped carbon nanodots	1.8	(34)
B, N, S-co-doped carbon dots	90.0	(35)
Graphene quantum dots	450.0	(36)
Octavinyl-polyhedral oligomeric silsesquioxane	0.9	(37)
3-aminopyridazine-functionalized rhodamine B	25.4	(38)
Indolizino[3,2-c]quinoline derivative	1000.0	(39)
Rhodamine B-based	12.8;11.0	(40)
2-methoxybenzylamine and 2-thiophenemethylamine		
2,2' thiobis (ethylamine)-functionalized 2-hydroxy 1-naphthaldehyde	300.0	(41)
Chemosensor T	0.178	This work

Furthermore, the detection mechanism of chemosensor **T** for Fe^{3+} and CN^- were investigated by FT-IR, Job' plot, SEM and the density functional theoretical (DFT). In the IR spectra of **T** and its complex (Figure S11), the stretching vibration absorption peaks of -OH and $\text{H}_3\text{C-O-}$ on chemosensor **T** appeared at 3408 cm^{-1} and 1274 cm^{-1} , respectively. Whereas the absorption peaks of -OH disappeared after the addition of 0.24 equiv. Fe^{3+} into **T** (forming the complex T-Fe^{3+}), and absorption peaks of $\text{H}_3\text{C-O-}$ was weakened. The results indicated that **T** coordinated with Fe^{3+} via O- Fe^{3+} -O coordination bonds. Subsequently, upon the addition of 5.0 equiv CN^- into the complex T-Fe^{3+} , the absorption peaks of -OH recovered to 3402 cm^{-1} , suggesting the existence of competitive coordination interaction between CN^- and T-Fe^{3+} . In addition, Job's plot analysis was implemented to evaluate the complexation behaviour

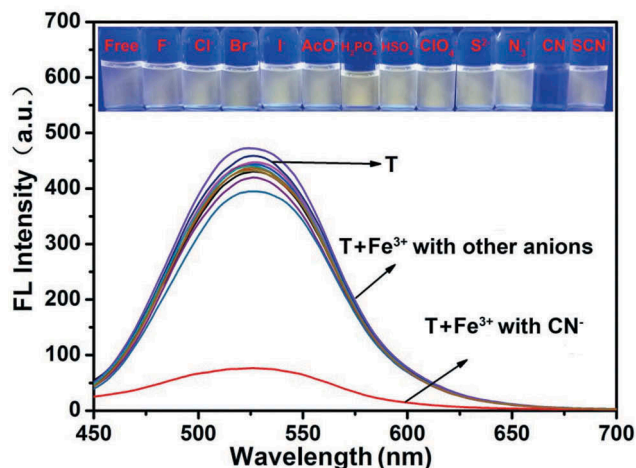


Figure 8. (colour online) Fluorescent emission spectra of T-Fe^{3+} ($2 \times 10^{-4}\text{ M}$) in DMSO/ H_2O (8: 2, v/v) binary solution in the presence of CN^- and other anions (5.0 equiv.) ($\lambda_{\text{ex}} = 390\text{ nm}$). Inset: Colour changes observed at UV lamp (365 nm) after 5.0 equiv. various anions were added into **T**.

between chemosensor **T** and Fe^{3+} . As shown in Figure S12, the inflexion point appeared at the mole fraction of 0.34, which demonstrated the binding mode of 2:1 between chemosensor **T** and Fe^{3+} . Moreover, the ESI-MS experiment was performed, as shown in the Figure S13, complex T-Fe^{3+} showed the peaks at $m/z = 259.98$ corresponding to $[\text{2T} + \text{Fe}^{3+} + \text{Na}^+]^{4+}$ after the appropriate amount of Fe^{3+} was added into **T** solution for forming complex T-Fe^{3+} , the result proved the 2:1 complexation stoichiometry between molecule **T** and Fe^{3+} , which further indicated the existence of coordination interactions between molecule **T** and Fe^{3+} .

Based on the above these results, we proposed the possible recognition mechanism of chemosensor **T** towards Fe^{3+} and CN^- . As shown in Scheme 1, in the absence of Fe^{3+} , the oxygen atom of methoxy of **T** could partially transfer an electron to the biphenyl (PET ON) (42, 43) and a hydroxyl proton could be transferred to a neighbouring methoxy oxygen along with the formation of intramolecular hydrogen bonds ($\text{OH} \dots \text{O}$), which led to a relative weak fluorescent emission at 528 nm. Upon the addition of Fe^{3+} into **T** solution (forming the complex T-Fe^{3+}), the oxygen atoms of hydroxyl and methoxy group participated in the coordination with Fe^{3+} , which destroyed intramolecular hydrogen bonds between hydroxyl and methoxy group, so that inhibited the PET process (PET OFF). Therefore, a remarkable fluorescence enhancement of **T** was induced by Fe^{3+} at 528 nm. After the addition of CN^- into T-Fe^{3+} , the coordination bonds of the complex T-Fe^{3+} were destroyed due to CN^- competitively bound to Fe^{3+} . Therefore, PET process (PET ON) and fluorescence of **T** were recovered.

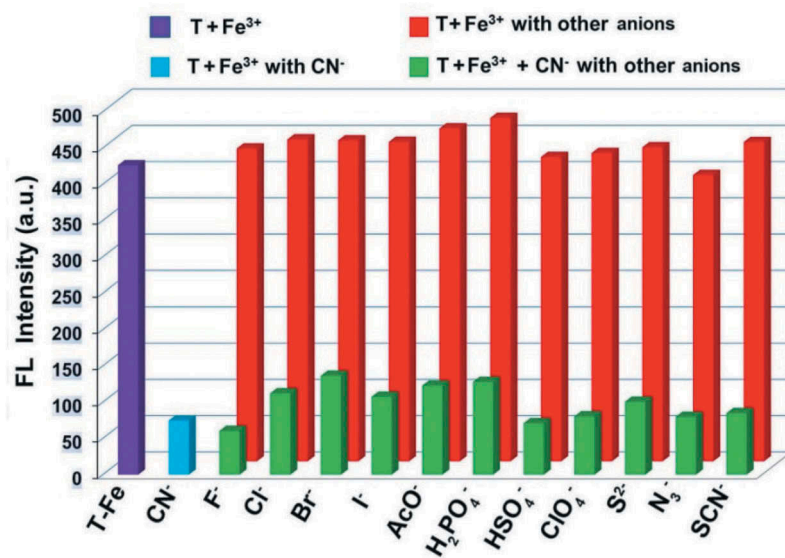
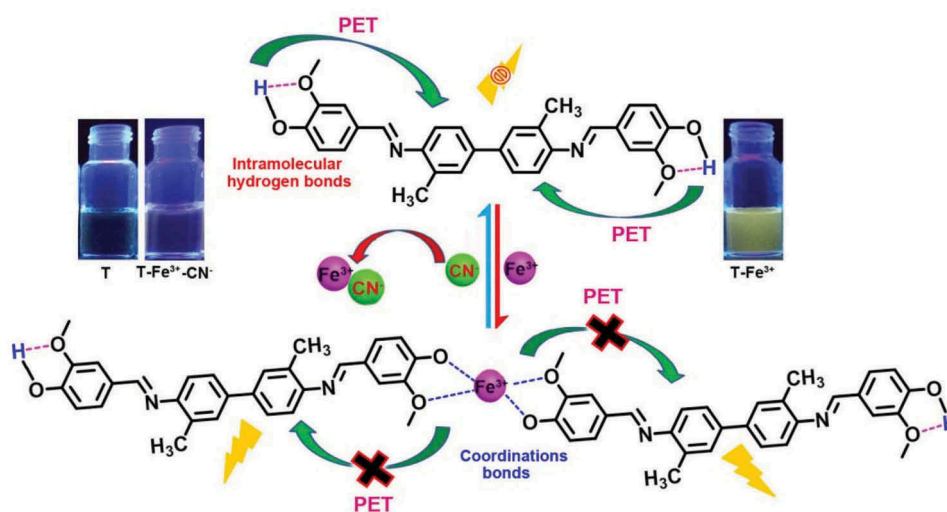


Figure 9. (colour online) Fluorescent histogram of **T-Fe³⁺** with addition of 5.0 equiv. **CN⁻** in the presence of various anions in DMSO/H₂O (8: 2, v/v) binary solution ($\lambda_{\text{ex}} = 390 \text{ nm}$, $\lambda_{\text{em}} = 528 \text{ nm}$).



Scheme 1. (colour online) The proposed detection mechanism of chemosensor **T** to **Fe³⁺** and **CN⁻**.

Subsequently, the SEM was also utilised for further investigating the morphological features of the powder **T** and its complex. As shown in Figure S14, the microstructure of **T** was blocky structure. However, the structure of **T** transformed into laminar microstructure after adding **Fe³⁺** into the **T**, which could be attribute to the complexation interaction between **T** and **Fe³⁺**. In addition, when **T-Fe³⁺** was treated with **CN⁻**, the laminar microstructure was transformed into a plicated microstructure, which could be caused by the competitive coordination interaction between **CN⁻** and **T-Fe³⁺**.

In order to further study the possible coordination interaction between **T** and **Fe³⁺**, the complex geometry of **T-Fe³⁺** was optimised by density functional theoretical

(DFT) calculations based on the theoretical level of B3LYP/6-31G (44), and the optimised structures of the ground state were shown in Figure S15. The orbital energies of the HOMO and LUMO of **T** and **T-Fe³⁺** were also obtained (Table S1). As shown in Figure 10, the energy gap between the HOMO and LUMO in **T** and **T-Fe³⁺** was calculated to be 3.68 eV and 3.21 eV, respectively. Decrease in the HOMO-LUMO energy gaps of **T** could stabilise the whole system after **T** coordinate with **Fe³⁺** (forming the complex **T-Fe³⁺**) (45), indicating the proposed coordination mechanism of **T** with **Fe³⁺** was rational.

The reversibility is a significant aspect for a chemosensor to be widely applied in the ionic and molecular detection field. Hence, the reversibility of chemosensor **T** was further

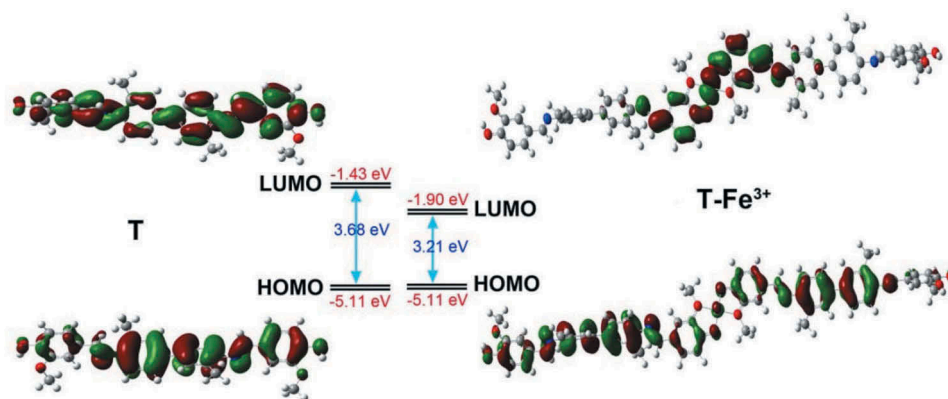


Figure 10. (colour online) HOMO and LUMO orbitals of **T**, T-Fe^{3+} .

investigated by alternating the addition of Fe^{3+} and CN^- into the **T** solution. Initially, **T** was induced to generate strong fluorescent emission after the addition of Fe^{3+} into **T** solution (forming the complex T-Fe^{3+}), which Fe^{3+} acts as an 'ON switch' in the detection process. Subsequently, with the addition of CN^- into the complex T-Fe^{3+} (forming the complex $\text{T-Fe}^{3+}\text{-CN}^-$), $\text{T-Fe}^{3+}\text{-CN}^-$ showed obvious fluorescence quenching by showing 'OFF' behaviour. The 'ON-OFF-ON' switching process could be repeated at least four times with little fluorescent efficiency loss (Figure S16). Therefore, these results not only verified **T** possessed excellent reversibility but also **T** could be used as excellent 'ON-OFF-ON' fluorescent switch (Figure S17).

Based on above the reversible property of **T**, **T** can switch between different fluorescent emission states, i.e. 'ON' (fluorescent enhancement) or 'OFF'

(fluorescent quenching), which showed 'Reading-Erasing-Writing-Reading' cyclic behaviour with the help of reversible IMPLICATION logic operations Figure 11(a-d). In the IMPLICATION logic gate, Fe^{3+} (Input 1) and CN^- (Input 2) are defined as two inputs, the presence of Fe^{3+} or CN^- could be defined as 1, the absence of Fe^{3+} or CN^- be defined as 0. Meanwhile, the fluorescent intensity of **T** at 528 nm was defined as the output signal, and fluorescent enhancement and fluorescent quenching of **T** were defined as 'state 1' and 'state 0', respectively. From the truth table in Fig. 14a-b, it could be observed that the presence of only Fe^{3+} (Input 1 = 1 and Input 2 = 0) induce a strong fluorescent emission implying that the output signal was above the threshold value (output = 0). However, other possible input combinations [(0, 0), (0, 1), and (1, 1)] could lead to the output signal below the threshold value, i.e. the output = 1. Therefore, an

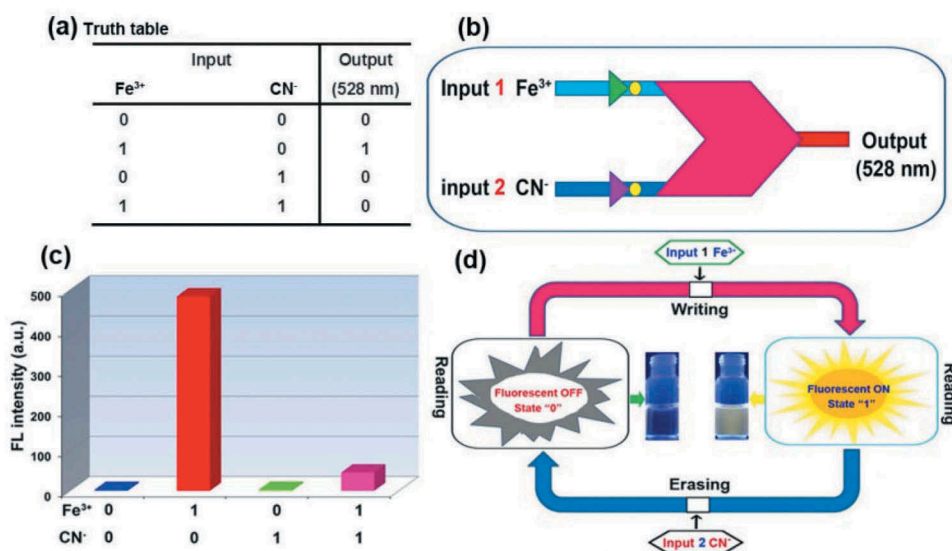


Figure 11. (colour online) (a) Truth table for the IMPLICATION logic gate; (b) IMPLICATION logic gate represented using a conventional gate notation; (c) Histogram of the output signals in presence of different inputs; (d) Feedback loop showing the reversible logic operations for the memory element with 'Reading-Erasing-Writing-Reading' functions.

IMPLICATION logic gate was successfully constructed by monitoring the fluorescent change of chemosensor **T** at 528 nm with the two inputs (Fe^{3+} and CN^-).

In order to further exploit the practical application of chemosensor **T**, the test papers and thin films were prepared. First, test papers were obtained by immersing the filter papers into **T** (1×10^{-2} M) DMSO/ H_2O (8: 2, v/v) binary solution and drying in air. Intriguingly, the test papers could serve as an efficient test kits for convenient detection of Fe^{3+} in water. As shown in Figure 12(b), these test papers exhibit weak fluorescence emission, upon the addition of different concentrations Fe^{3+} water solution (from 1.0 M to 1×10^{-10} M) into the test papers, the test papers exhibited distinct fluorescence response for Fe^{3+} . The lowest response concentration of these test papers to Fe^{3+} was 10^{-9} M.

In addition, the thin films were also prepared by loading **T** (DMSO/ H_2O , 1×10^{-2} M) binary solution on the silica plate and dried in air. As shown in Figure 12(a), the thin films exhibited weak fluorescence under the irradiation of UV lamp (365 nm). However, when writing on the films with a capillary tube dipping in Fe^{3+} water solution, a bright yellow fluorescent writing trace appeared and

the bright yellow writing trace could be erased by brushing CN^- on the film again. Therefore, the thin films based on chemosensor **T** could act as convenient and reproducible fluorescent security display materials.

Conclusion

To sum up, we have successfully developed a colourimetric and fluorescent dual-channel chemosensor **T** based on double schiff-base. Interestingly, **T** could selectively detect Fe^{3+} via fluorescent 'turn-on' response and the fluorescent spectrum detection limit of **T** towards Fe^{3+} was 0.178 nM. Simultaneously, upon the addition of Fe^{3+} into **T** solution, **T** showed an obvious colour change from pale yellow to colourless. In addition, **T** could also alternately detect CN^- . Next, the fluorescent 'ON-OFF-ON' responding circle also was constructed, which could be repeated over 4 times by the successive addition of Fe^{3+} and CN^- into **T**. The fluorescent 'ON-OFF-ON' responding circle was utilised as an IMPLICATION logic gate at the molecular level. Finally, the test papers and films loading **T** were prepared, which could be used as a fluorescent display material for the detection

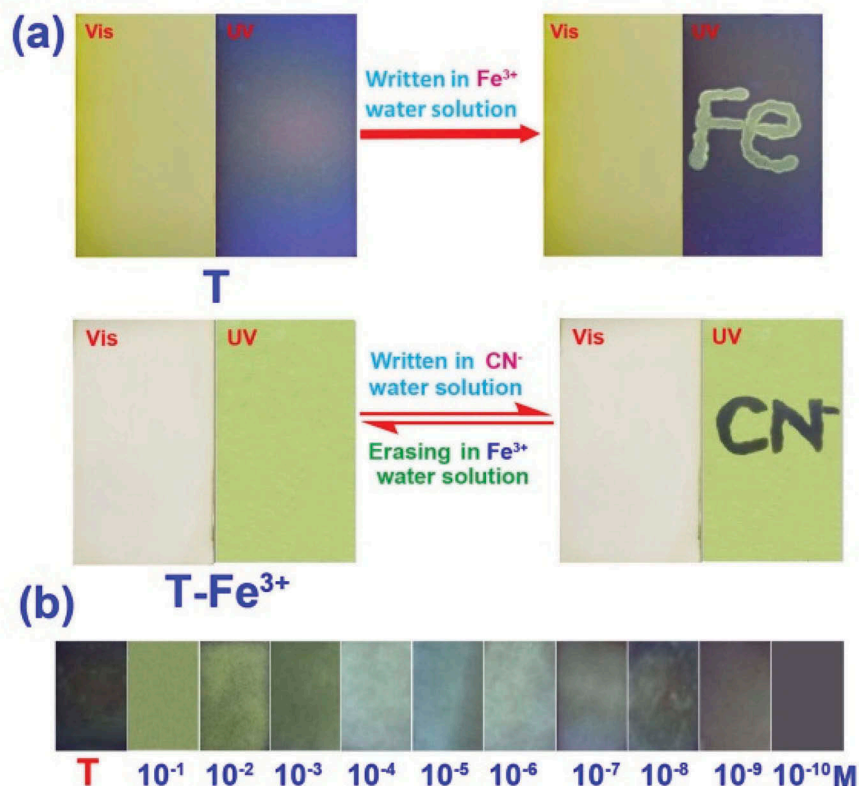


Figure 12. (colour online) (a) Photos of the silica gel plates loaded with **T** or **T-Fe³⁺** were used to detect Fe^{3+} and CN^- in aqueous solutions under UV lamp at 365 nm; (b) Fluorescent colour changes (under the UV lamp, at 365 nm) of **T** based on test kit after addition of various concentration Fe^{3+} aqueous solutions (from 0 M to 1×10^{-10} M).

of Fe³⁺ and CN⁻. This work will be of great value in ion recognition, environmental monitoring and smart materials.

Disclosure statement

No potential conflict of interest was reported by the authors.

Funding

This work was supported by The National Natural Science Foundation of China (NSFC) (No. 21574104; 21662031; 21661028).

References

- Deng, D.D.; Yang, H.; Liu, C.; Zhao, K.; Li, J.G.; Deng, A.P. *Food Chem.* **2019**, *277*, 595–603. DOI: [10.1016/j.foodchem.2018.10.129](https://doi.org/10.1016/j.foodchem.2018.10.129).
- Zhang, G.X.; Ji, R.X.; Kong, X.Y.; Ning, F.J.; Liu, A.K.; Cui, J. C.; Ge, Y.Q. *RSC Adv.* **2019**, *9*, 1147–1150. DOI: [10.1039/C8RA08967A](https://doi.org/10.1039/C8RA08967A).
- Zhou, J.W.; Zou, X.M.; Song, S.H.; Chen, G.H. *J. Agric. Food Chem.* **2018**, *66*, 1307–1319. DOI: [10.1021/acs.jafc.7b05119](https://doi.org/10.1021/acs.jafc.7b05119).
- Prince, A.C.; Aditi Jani, A.; Korb, M.; Tipirneni, K.E.; Kasten, B.B.; Rosenthal, E.L.; Warram, J.M. *J. Surg. Oncol.* **2017**, *116*, 898–906. DOI: [10.1002/jso.24733](https://doi.org/10.1002/jso.24733).
- Bruno, J.G.; Sivills, J.C.; Phillips, T. *J. AOAC Int.* **2017**, *100*, 895–899. DOI: [10.5740/jaoacint.17-0163](https://doi.org/10.5740/jaoacint.17-0163).
- Chauhan, B.; Jalalpure, S. *Pharm. Methods.* **2016**, *7*, 99–103. DOI: [10.5530/phm.2016.7.15](https://doi.org/10.5530/phm.2016.7.15).
- Mauk, M.; Song, J.Z.; Bau, H.H.; Gross, R.; Bushman, F.D.; Collman, R.G.; Liu, C.C. *Lab. Chip.* **2017**, *17*, 382–394. DOI: [10.1039/C6LC01239F](https://doi.org/10.1039/C6LC01239F).
- Kim, J.; Campbell, A.S.; Wang, J. *Talanta.* **2018**, *177*, 163–170. DOI: [10.1016/j.talanta.2017.08.077](https://doi.org/10.1016/j.talanta.2017.08.077).
- Scirica, B.M.; *Clin. Chem.* **2017**, *63*, 186–195. DOI: [10.1373/clinchem.2016.255539](https://doi.org/10.1373/clinchem.2016.255539).
- Zhao, F.; Zhou, X.Y.; Liu, Y.; Shi, Y.; Dai, Y.F.; Yu, G.H. *Adv. Mater.* **2019**, *31*, 1806446–1806452. DOI: [10.1002/adma.201806446](https://doi.org/10.1002/adma.201806446).
- Li, X.; Li, Z.; Yang, Y.W. *Adv. Mater.* **2018**, *30*, 1800177–1800183. DOI: [10.1002/adma.201800177](https://doi.org/10.1002/adma.201800177).
- Mirica, K.A.; Azzarelli, J.M.; Weis, J.G.; Schnorr, J.M.; Swager, T.M. *Proc. Natl. Acad. Sci. U. S. A.* **2013**, *110*, E3265–E3270. DOI: [10.1073/pnas.1307251110](https://doi.org/10.1073/pnas.1307251110).
- Jayawardane, B.M.; McKelvie, I.D.; Kolev, S.D. *Anal. Chem.* **2015**, *87*, 4621–4626. DOI: [10.1021/acs.analchem.5b00125](https://doi.org/10.1021/acs.analchem.5b00125).
- Lim, S.H.; Feng, L.; Kemling, J.W.; Musto, C.J.; Suslick, K.S. *Nat. Chem.* **2009**, *1*, 562–567. DOI: [10.1038/nchem.360](https://doi.org/10.1038/nchem.360).
- Prasad, R.M.; Lauterbach, S.; Kleebe, H.-J.; Merdrignac-Conanec, O.; Barsan, N.; Weimar, U.; Gurlo, A. *ACS Sens.* **2017**, *2*, 713–717. DOI: [10.1021/acssensors.7b00064](https://doi.org/10.1021/acssensors.7b00064).
- Su, S.; Wu, W.H.; Gao, J.M.; Lu, J.X.; Fan, C.H. *J. Mater. Chem.* **2012**, *22*, 18101–18110. DOI: [10.1039/c2jm33284a](https://doi.org/10.1039/c2jm33284a).
- Lin, Z.T.; Li, Y.X.; Gu, J.H.; Wang, H.E.; Zhu, Z.; Hong, X.; Zhang, Z.J.; Lu, Q.Q.; Qiu, J.Y.; Wang, X.F.; Bao, J.M.; Wu, T. F. *Adv. Funct. Mater.* **2018**, *28*, 1802482–1802492. DOI: [10.1002/adfm.201802482](https://doi.org/10.1002/adfm.201802482).
- Sarkar, A.; Chakraborty, S.; Lohar, S.; Ahmmmed, E.; Saha, N.C.; Mandal, S.K.; Dhara, K.; Chattopadhyay, P. *Chem. Res. Toxicol.* **2019**, *32*, 1144–1150. DOI: [10.1021/acs.chemrestox.9b00005](https://doi.org/10.1021/acs.chemrestox.9b00005).
- Zhu, H.; Peck, S.C.; Bonnot, F.; van der Donk, W.A.; Klinman, J.P. *J. Am. Chem. Soc.* **2015**, *137*, 10448–10451. DOI: [10.1021/jacs.5b03907](https://doi.org/10.1021/jacs.5b03907).
- Basoglu, A.; Tosun, G.; Ocak, M.; Alp, H.; Yayli, N.; Ocak, U. *J. Agric. Food Chem.* **2015**, *63*, 2654–2659. DOI: [10.1021/jf505336d](https://doi.org/10.1021/jf505336d).
- Ebrahimi, K.H.; Hagedoorn, P.L.; Hagen, W.R. *Chem. Rev.* **2015**, *115*, 295–326. DOI: [10.1021/cr5004908](https://doi.org/10.1021/cr5004908).
- Rouault, T.A.; *Nat. Chem. Biol.* **2006**, *2*, 406–414. DOI: [10.1038/nchembio807](https://doi.org/10.1038/nchembio807).
- D'Autreaux, B.; Tucker, N.P.; Dixon, R.; Spiro, S. *Nature.* **2005**, *437*, 769–772. DOI: [10.1038/nature03953](https://doi.org/10.1038/nature03953).
- Haehling, S.V.; Jankowska, E.A.; van Veldhuisen, D.J.; Ponikowski, P.; Anker, S.D. *Nat. Rev. Cardiol.* **2015**, *12*, 659–669. DOI: [10.1038/nrcardio.2015.109](https://doi.org/10.1038/nrcardio.2015.109).
- Lopez, A.; Cacoub, P.; Macdougall, I.C.; Peyrin-Biroulet, L. *Seminars.* **2016**, *387*, 907–916.
- Wu, J.S.; Liu, W.M.; Ge, J.C.; Zhang, H.Y.; Wang, P.F. *Chem. Soc. Rev.* **2011**, *40*, 3483–3495. DOI: [10.1039/c0cs00224k](https://doi.org/10.1039/c0cs00224k).
- Jung, K.H.; Lee, K.H. *Anal. Chem.* **2015**, *87*, 9308–9314. DOI: [10.1021/acs.analchem.5b01982](https://doi.org/10.1021/acs.analchem.5b01982).
- Kim, H.J.; Ko, K.C.; Lee, J.H.; Lee, J.Y.; Kim, J.S. *Chem. Commun.* **2011**, *47*, 2886–2888. DOI: [10.1039/c0cc05018k](https://doi.org/10.1039/c0cc05018k).
- Lin, Q.; Jiang, X.M.; Ma, X.Q.; Liu, J.; Yao, H.; Zhang, Y.M.; Wei, T.B. *Sens. Actuators B.* **2018**, *272*, 139–145. DOI: [10.1016/j.snb.2018.05.094](https://doi.org/10.1016/j.snb.2018.05.094).
- Lin, Q.; Fan, Y.Q.; Gong, G.F.; Mao, P.P.; Wang, J.; Guan, X. W.; Liu, J.; Zhang, Y.M.; Yao, H.; Wei, T.B. *Sustainable Chem. Eng.* **2018**, *6*, 8775–8781. DOI: [10.1021/acssuschemeng.8b01124](https://doi.org/10.1021/acssuschemeng.8b01124).
- Zhang, Y.M.; Zhu, W.; Huang, X.J.; Qu, W.J.; He, J.X.; Fang, H.; Yao, H.; Wei, T.B.; Lin, Q. *Sustainable Chem. Eng.* **2018**, *6*, 16597–16606. DOI: [10.1021/acssuschemeng.8b03824](https://doi.org/10.1021/acssuschemeng.8b03824).
- Shi, B.B.; Liu, Y.Z.; Zhu, H.T.Z.; Vanderlinden, R.T.; Shangguan, L.Q.; Ni, R.D.; Acharyya, K.; Tang, J.H.; Zhou, Z.X.; Li, X.P.; Huang, F.H.; Sang, P.J. *J. Am. Chem. Soc.* **2019**, *141*, 6494–6498. DOI: [10.1021/jacs.9b02281](https://doi.org/10.1021/jacs.9b02281).
- Shangguan, J.F.; Huang, J.; He, D.G.; He, X.X.; Wang, K.M.; Ye, R.Z.; Yang, X.; Qing, T.P.; Tang, J.L. *Anal. Chem.* **2017**, *89*, 7477–7484. DOI: [10.1021/acs.analchem.7b01053](https://doi.org/10.1021/acs.analchem.7b01053).
- Shi, B.F.; Su, Y.B.; Zhang, L.L.; Huang, M.J.; Liu, R.J.; Zhao, S.L. *ACS Appl. Mater. Interfaces.* **2016**, *8*, 10717–10725. DOI: [10.1021/acsami.6b01325](https://doi.org/10.1021/acsami.6b01325).
- Liu, Y.H.; Duan, W.X.; Song, W.; Liu, J.J.; Ren, C.L.; Wu, J.; Liu, D.; Chen, H.L. *ACS Appl. Mater. Interfaces.* **2017**, *9*, 12663–12672.
- Zhu, X.W.; Zhang, Z.; Xue, Z.J.; Huang, C.H.; Shan, Y.; Liu, C.; Qin, X.Y.; Yang, W.S.; Chen, X.; Wang, T. *Anal.*

- Chem.* **2017**, *89*, 12054–12058. DOI: [10.1021/acs.analchem.7b02499](https://doi.org/10.1021/acs.analchem.7b02499).
- (37) Omer, N.; Zhang, F.Y.; Zhao, G.; Guang, S.Y.; Xu, H.Y. *Analyst.* **2019**, *144*, 3414–3421. DOI: [10.1039/C9AN00070D](https://doi.org/10.1039/C9AN00070D).
- (38) Cheng, Z.; Zheng, L.; Xu, H.; Pang, L.; He, H. *Anal. Methods.* **2019**, *11*, 2565–2570. DOI: [10.1039/C9AY00499H](https://doi.org/10.1039/C9AY00499H).
- (39) Lim, B.; Baek, B.; Jang, K.; Lee, N.K.; Lee, J.H.; Lee, Y.; Kim, J.; Kang, S.W.; Park, J.; Kim, S.; Kang, N.W.; Hong, S.; Kim, D.D.; Kim, I.; Hwang, H.; Lee, J. *Dyes Pigm.* **2019**, *169*, 51–59. DOI: [10.1016/j.dyepig.2019.05.008](https://doi.org/10.1016/j.dyepig.2019.05.008).
- (40) Wu, Z.Y.; Xu, Z.Y.; Tan, H.Y.; Li, X.; Yan, J.W.; Dong, C.Z.; Zhang, L. *Spectrochim. Acta Part A.* **2019**, *213*, 167–175. DOI: [10.1016/j.saa.2019.01.032](https://doi.org/10.1016/j.saa.2019.01.032).
- (41) Lee, S.Y.; Yang, M.; Kim, C. *Spectrochim. Acta Part A.* **2018**, *205*, 622–629. DOI: [10.1016/j.saa.2018.07.091](https://doi.org/10.1016/j.saa.2018.07.091).
- (42) Asthana, S.K.; Kumar, A.; Neeraj,; Shweta,; Hira, S.K.; Manna, P.P.; Upadhyay, K.K. *Inorg. Chem.* **2017**, *56*, 3315–3323. DOI: [10.1021/acs.inorgchem.6b02752](https://doi.org/10.1021/acs.inorgchem.6b02752).
- (43) Gupta, A.S.; Paul, K.; Luxami, V. *Anal. Methods.* **2018**, *10*, 983–990. DOI: [10.1039/C7AY02779F](https://doi.org/10.1039/C7AY02779F).
- (44) Bao, X.F.; Shi, J.X.; Nie, X.M.; Zhou, B.J.; Wang, X.L.; Zhang, L.Y.; Liao, H.; Pang, T. *Bioorg. Med. Chem.* **2014**, *22*, 4826–4835. DOI: [10.1016/j.bmc.2014.06.054](https://doi.org/10.1016/j.bmc.2014.06.054).
- (45) Wang, Y.; Chang, H.Q.; Wu, W.N.; Zhao, X.L.; Yang, Y.; Xu, Z.Q.; Xu, Z.H.; Jia, L. *Sens. Actuators B.* **2017**, *239*, 60–68. DOI: [10.1016/j.snb.2016.07.170](https://doi.org/10.1016/j.snb.2016.07.170).